Proceedings of the 28th IEEE
EMBS Annual International Conference
New York City, USA, Aug 30-Sept 3, 2006

A New Multimodal Imaging Strategy for integrating fMRI with EEG

Zhongming Liu, *Student Member, IEEE,* Bin He, *Fellow, IEEE*

Abstract*—For the multimodal functional neuroimaging combining fMRI and EEG, it is of significance to correct the distortion due to the fMRI-EEG mismatches, which arise from the fundamental difference between brain electric and hemodynamic activities. In the present study, we proposed a novel two-step approach (referred to as "Twomey algorithm") for the fMRI-constrained cortical source imaging. In the first step, a "hard" spatial prior derived from the fMRI was imposed to solve the EEG inverse problem with a reduced source space; in the second step, the fMRI constraint was removed and the source estimate from the first step was re-entered as the initial guess of the desired solution into an EEG least squares fitting procedure with Twomey regularization. We evaluated the performance of Twomey algorithm in comparison with the well-known 90% fMRI-constrained Wiener filter and the EEG-alone weighted minimum norm methods in a randomized computer simulation setting. We examined the effects of invalid fMRI priors including fMRI invisible sources, fMRI extra regions and fMRI displacement. The present results in terms of the point spread function (PSF) and the localization error (LE), demonstrated that 1) relative to the EEG-alone solution, a higher spatial resolution can be achieved by using the fMRI priors in cortical source imaging; 2) the occurrence of fMRI invisible sources is the most problematic factor responsible for the error of the fMRI-EEG integrated cortical source imaging; and 3) the Twomey algorithm is more robust than the Wiener filter approach under invalid fMRI priors. The proposed Twomey approach may make an important contribution to the multimodal neuroimaging integrating fMRI with EEG.

I. Introduction

Both functional magnetic resonance imaging (fMRI) and electroencephalography (EEG) are the widely used tools to study the human brain function. Functional MRI, through measuring the regional hemodynamic change, is capable of localizing the "activated" brain regions with a high spatial resolution in a millimeter scale [1,2]. However, the sluggishness of hemodynamic response limits the use of fMRI to study the temporal aspect of rapidly changing neural activities. To the contrary, neural activities generate the instantaneous change of the external electrical potential field measurable by EEG through recordings from an array of sensors placed on the scalp; therefore EEG provides excellent temporal resolution. However, due to the lack of a physical mechanism (e.g. spatial encoding in MRI/fMRI) to spatially separate the source signals that contribute to the generation of scalp potentials, the EEG-based functional imaging faces a technical difficulty of solving a highly ill-posed "inverse problem", in order to infer the locations of the electrical sources from EEG measurements.

Nevertheless, the complementary nature and feasibility of recording fMRI and EEG simultaneously have recently attracted great interest in integrating these two modalities, in an attempt to achieve high resolutions in both spatial and temporal domains [3]. For the focalized fMRI activations, a short-window time course can be obtained for each activated region, by placing multiple current dipoles around the fMRI activations and fitting the dipole parameters to the measured EEG signals instant by instant [4]. A more generalized approach is the use of fMRI activations as spatial priors for imaging the continuous cortical distribution of current density from the instantaneous EEG signals. This method, namely the fMRI-constrained cortical source imaging, implies that the activated fMRI voxels are more likely to be the EEG sources than other cortical locations [5, 6].

Although the fMRI-constrained cortical source imaging has a sound physiological basis, it is still important to consider possible mismatches between multi-modal signals, such as the presence of fMRI extra sources, fMRI invisible sources and displacement of fMRI activation from electrical current sources. The fMRI extra sources are referred to the fMRI activations that produce no observable EEG/MEG signals at the instant of interest. The fMRI invisible sources are the generators of bioelectrical signals that are not detected by fMRI. Additionally, the possible difference in the locations of synaptic electrical activity and the involved vessels can cause slight displacement of fMRI "hotspots" away from neural electrical generators [7].

To deal with fMRI-EEG (or MEG) mismatches, previous studies suggested using fMRI partial constraint (e.g. 90% fMRI weighting) [5]. In the present study, we proposed an alternative algorithm using Twomey regularization [8] to correct the distortion due to invalid fMRI priors. The proposed algorithm consists of two steps. In the first step, a "hard" spatial prior derived from fMRI was imposed to solve the EEG inverse problem with a reduced source space; in the second step, the fMRI constraint was removed and the source estimate from the first step was re-entered as the initial guess of the desired solution into an EEG least square fitting procedure with Twomey regularization [9].

II. Methods

A. EEG-based Cortical Source Imaging

To model the distributed electrical activity, several

This work was supported in part by NSF BES-0411480, NIH RO1 EB-00178, and the BME Institute of the University of Minnesota.

Zhongming Liu is with the Department of Biomedical Engineering at the University of Minnesota (zmliu@umn.edu).

Bin He is with the Department of Biomedical Engineering at the University of Minnesota (binhe@umn.edu).

thousands current dipoles are evenly placed on the cortical surface [10]. The electrical potential generated by any unitary current dipole can be accurately calculated by boundary element method (BEM), utilizing a three-layer triangulated head model [11]. Under the quasi-static condition, any scalp potential distribution is expressed as a linear superimposition of the contribution from all of the dipole sources plus additive noise, as Eq. (1).

$$\Phi = LJ + b \tag{1}$$

where Φ is the vector of instantaneous EEG recordings, J is the vector of unknown dipole moments, b is the noise vector, and L is the transfer matrix.

Accordingly, the cortical source imaging, stated as an EEG inverse problem, is to estimate the magnitudes of all of the current dipoles from the EEG recordings. To overcome the ill-posedness of the inverse problem, additional constraints must be imposed to obtain a unique solution. Figure 1 illustrates an example of cortical source model, BEM model and the EEG source imaging result.

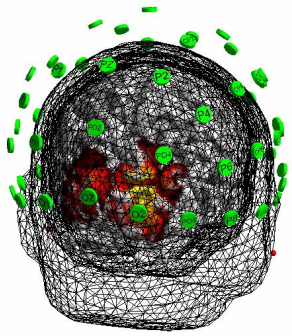

Fig.1. Illustration of the EEG-based cortical source imaging.

B. *fMRI-EEG integrated cortical source imaging*

The Twomey algorithm for the fMRI-EEG integration consists of two steps. In the first step, a "hard" fMRI constraint is imposed by constructing a diagonal source covariance matrix R_f from fMRI. As illustrated in Figure 2, the diagonal element of R_f that corresponds to any source location within an fMRI activation is set to a weight factor f ($f>1$), otherwise 1. By setting f as a dominantly large value (e.g. f=100), the fMRI-derived source covariance matrix effectively reduces the EEG source space to the fMRI active region, while all of the other non-fMRI locations are highly penalized. As a result, the source reconstruction J^{fMRI}, as in Eq. (2), has a spatial resolution as high as fMRI.

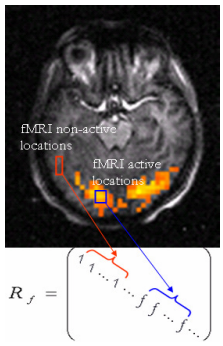

Fig.2. Illustration of fMRI-derived cortical source covariance matrix.

$$J^{fMRI} = T^{fMRI}\Phi,\ T^{fMRI} = rR_f L^T\left(rLR_f L^T + C\right)^{-1} \tag{2}$$

where r is the regularization parameter which can be determined by the "L-curve" method [12] and C is the noise covariance matrix estimated from the EEG data itself.

As would be expected, such an overconstrained high-resolution cortical source reconstruction is highly sensitive to invalid fMRI priors. To overcome the resulting distortion in the second step, J^{fMRI} is re-entered as an initial estimate into the EEG least square fitting procedure with Twomey regularization [8], which minimizes the difference between the desired solution $\hat{J}$ and a rough estimate J^{fMRI}. The Twomey regularized solution can be written as (3)

$$\arg\min_J\left(\left\|C^{-1/2}(LJ-\Phi)\right\|^2 + \lambda\left\|J - J^{fMRI}\right\|^2\right) \tag{3}$$

Here, the weighting matrix $C^{-1/2}$ is still introduced to compensate for different levels of noise contamination in the sensor space. To minimize (3), the solution tends to shift away from J^{fMRI} in a way to reduce the residual error of EEG data fitting. Again, λ in (3) can be obtained by the "L-curve" method [12]. Consequently, the solution to (3) is

$$J^{Twomey} = J^{fMRI} + L^T\left(LL^T + \lambda C\right)^{-1}\left(\Phi - LJ^{fMRI}\right) \tag{4}$$

where $J^{fMRI} = T^{fMRI}\Phi$. From (4), the Twomey solution can be interpreted as the fMRI overconstrained solution J^{fMRI} plus a data-driven correction term which is a minimum norm projection of the data that is not explained by J^{fMRI}. In fact, this solution is still a linear inverse solution and the inverse operator can be written as (5):

$$T^{Twomey} = T^{fMRI} + L^T\left(LL^T + \lambda C\right)^{-1}\left(I - LT^{fMRI}\right) \tag{5}$$

C. *Computer Simulation*

Through computer simulation, the performance of the proposed method, abbreviated as *Twomey*, was examined in comparison with weighted minimum norm [13] and the well-known 90% fMRI-constrained Wiener estimation [5], denoted as *WMN* and *Wiener*, respectively.

The simulation was based on randomized placement of unitary dipole sources and synthetic fMRI activations in consideration of three types of fMRI-EEG mismatches: fMRI invisible sources, fMRI extra sources and fMRI displacement. The instantaneous EEG measurements at 128 channels were generated through forward calculation with additive Gaussian white noise at SNR=5. The random source placement was repeated for 100 times for each simulation condition.

For fMRI invisible and extra sources, a measure of estimation error defined as "point spread function" (PSF) can be calculated for any source location [14]. Mathematically,

$$\rho_i^2 = \sum_{j\neq i}\left|(TL)_{ji}\right|^2 \Big/ \left|(TL)_{ii}\right|^2 \tag{6}$$

where $(TL)_{ji}$ describes the sensitivity of the estimate at a location j to activity at location i.

For fMRI displacement, "localization error" (LE) was calculated as distance between the location of the current dipole and the center of gravity of the source estimate. The reconstructed source image was thresholded such that 80% of the power of the estimated sources was remained.

III. Results

Fig. 3 shows two examples of cortical source imaging from 128-channel EEG data simulated at SNR=5 using three different inverse algorithms (WMN, Wiener and Twomey).

The upper row shows an example with five unitary dipole sources (Fig.3.A). The fMRI activation covered three sources, leaving the other two sources (marked by blue dotted circles) to behave as fMRI missing sources (Fig.3.C). WMN resulted in extended cortical source reconstruction (Fig.3.B) and ambiguity of localizing the simulated "true" sources. With valid fMRI priors, the 90% fMRI-constrained Wiener estimation substantially improved the spatial resolution of imaging fMRI visible sources; however the fMRI invisible sources were considerably underestimated (Fig.3.D). In contrast, the Twomey solution exhibited high-resolution reconstruction of the fMRI visible sources comparable to Wiener estimate, and it also remarkably accentuated and improved the estimation of activity

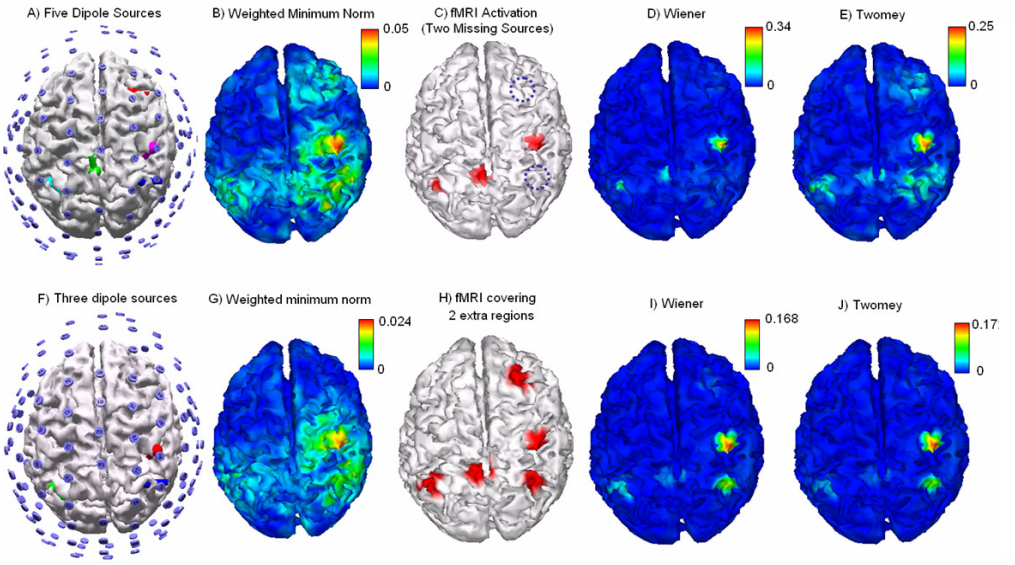

Fig. 3. Typical examples of effects of fMRI invisible and fMRI extra sources on three cortical source imaging methods: EEG-alone weighted minimum norm, 90% fMRI-constrained Wiener filter and Twomey algorithm. The upper row shows the results of simulation on fMRI invisible sources; the lower for fMRI extra sources.

associated with the fMRI invisible sources (Fig.3.E). This example demonstrated the efficacy of Twomey algorithm in revealing fMRI invisible sources.

The lower row shows an example with three unitary dipole sources (Fig.3.F). Except covering all of these three sources, the fMRI activation included two more extra regions without EEG sources (Fig.3.H). Similar as the first example, WMN solution had low resolution (Fig.3.G). For both Wiener and Twomey solutions, the fMRI visible sources maintained a high-resolution reconstruction. However, in Wiener solution slightly spurious sources appeared in the extra fMRI regions (Fig.3.I). By use of Twomey algorithm, the spurious sources induced by the fMRI extra areas appeared with smaller intensity in the reconstructed cortical source image (Fig.3.J). This example demonstrated that the fMRI extra sources did not significantly distort the fMRI-EEG integrated cortical imaging using either the new Twomey algorithm or the 90% fMRI-constrained Wiener filter approach. The slightly spurious sources that may occur within the extra fMRI regions for the Wiener filter approach can be further suppressed by using the alternative Twomey algorithm.

Fig. 4 shows the PSF values for all three algorithms (WMN, Wiener and Twomey) in 100 random trials with 5 unitary point sources and SNR=5. The simulated fMRI activations covered 4 sources, leaving one source to behave as an fMRI missing source. Fig. 4.A) shows the mean PSF averaged over the four fMRI visible sources in each trial. Clearly, both Wiener and Twomey resulted in much smaller PSF of fMRI visible sources than WMN. However, for the fMRI invisible source (as shown in Fig. 4.B), considerably larger PSF was found for Wiener than for WMN. The values of PSF of the fMRI invisible source for Twomey was much smaller than those for Wiener, and in many trials they were even smaller (or at least comparable) than WMN solution. Fig. 4.C) illustrates the PSF of the fMRI invisible source for both Wiener and Twomey algorithms as a function of the respective PSF value in WMN solution in the same trial. Clearly, as for the fMRI invisible sources that were more "visible" (with smaller PSF values) in WMN solution, it was more obvious to observe the improvement by use of Twomey algorithm relative to Wiener. If the fMRI invisible sources could hardly be imaged even in non-fMRI-biased WMN solution, Twomey algorithm was also less helpful in revealing such fMRI-missed sources.

Fig. 5 summarizes the effects of displacement of fMRI active region relative to the associated electric current dipole source on the localization error of fMRI-EEG integrated imaging approaches (Wiener and Twomey), in comparison with EEG-alone WMN solution. The bars in Fig. 3 represent the mean LE averaged over 100 random, with or without different levels of fMRI displacement (5, 10, 15 or 20 mm). The WMN solution had a mean localization error around 1-cm, and the error tended to decrease with higher SNR. With accurate fMRI priors, the fMRI-constrained solutions in both Wiener and Twomey had much smaller mean LE (about 4 to 5-mm) than WMN, and Wiener gave slightly smaller LE than Twomey. If the fMRI activation was displaced away from the electrical source, the LEs for both Wiener and Twomey increased when the displacement was enlarged. With a smaller fMRI displacement (e.g. 5-mm), the LEs for

Wiener and Twomey were very close, whereas with a relatively larger fMRI displacement (e.g. >1.0cm), Twomey

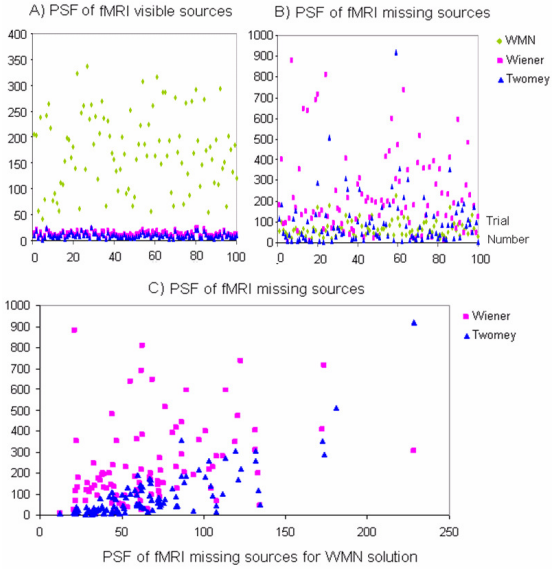

Fig. 4. The values of Point Spread Function (PSF) for either fMRI visible sources or fMRI invisible sources in 100 random trials.

gave smaller LE than Wiener. Moreover, even with the fMRI displacement as large as 2-cm, Wiener and Twomey still had smaller LE than WMN solution, except at SNR=10 Wiener had larger LE than WMN. This finding suggests that the incorporation of fMRI spatial prior even with less than 2-cm displacement was still helpful to localize the electrical sources, compared to the EEG-alone WMN solution.

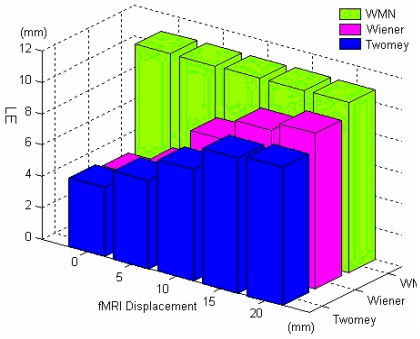

Fig. 5. The average localization error as a function of METHODS (Twomey, Wiener and WMN) and fMRI displacement (distance of fMRI activation away from the electrical source)

IV. DISCUSSION AND CONCLUSIONS

We have developed a new multimodal Twomey algorithm to integrate fMRI and EEG for cortical source imaging. The performance of the proposed Twomey algorithm has been evaluated via a series of computer simulation. The present results demonstrate that 1) relative to EEG-alone solution, higher spatial resolution can be achieved by using fMRI priors in cortical source imaging; 2) the occurrence of fMRI invisible sources is the most problematic factor that induced the error of fMRI-EEG integrated cortical source imaging; 3) under invalid fMRI priors, the Twomey algorithm provides better performance than the 90% fMRI-constrained Wiener filter approach.

In order to accurately integrate the fMRI and EEG/MEG, it is important to better understand and quantitatively model the coupling between electrophysiological and fMRI signals with the underlying neural activities. However, at the current stage when such a quantitative relationship between these signals are not yet well established, our proposed Twomey algorithm represents a contributive advancement over the conventional approach (90% fMRI weighted Wiener filter approach) to achieve high resolution spatiotemporal mapping with improved robustness against the presence of invalid fMRI prior information.

REFERENCES

[1] S. Ogawa, D. W. Tank, R. Menon, J. M. Ellermann, S-G Kim, H. Merkle and K Ugurbil, "Intrinsic signal changes accompanying sensory stimulation: functional brain mapping with magnetic resonance imaging," *Proc. Natl. Acad. Sci. USA*, vol. 89, pp. 5951-5955, 1992.

[2] K. K. Kwong, J. W. Belliveau, D. A. Chesler, I. E. Goldberg, R. M. Weisskoff, B. P. Poncelet, D. N. Kennedy, B. E. Hoppel, M. S. Cohen, R. Turner, H-M Cheng, T. J. Brady and B. R. Rosen, "Dynamic magnetic resonance imaging of human brain activity during primary sensory stimulation," *Proc. Natl. Acad. Sci. USA*, vol. 89, pp. 5675-5679, 1992.

[3] B. He and J. Lian, "High-resolution spatio-temporal functional neuroimaging of brain activity," *Crit. Rev. Biomed. Eng.,* vol. 30, pp. 283-306, 2002.

[4] S. P. Ahlfors, G. V. Simpson, A. M. Dale, J. W. Belliveau, A. K. Liu, A. Korvenoja, J. Virtanen, M. Huotilainen, R. B. H. Tootell, H. J. Aronen and R. J. Ilmoniemi, "Spatiotemporal activity of a cortical network for processing visual motion revealed by MEG and fMRI," *J Neurophysiol.*, vol. 82, 2545-2555, 1999.

[5] A. K. Liu, J. W. Belliveau, A. M. Dale, "Spatiotemporal imaging of human brain activity functional MRI constrained magnetoencephalography data: Monte Carlo simulations," *Proc. Natl. Acad. Sci. USA.*, vol. 95, 8945-8950, 1998.

[6] F. Babiloni, C. Babiloni, F..Carducci, F. Cincotti, L. Astolfi, A. Basilisco, P. M. Rossini, L. Ding, Y. Ni, J. Cheng, K. Christine, J. Sweeney and B. He: "Estimation of the cortical functional connectivity with the multimodal integration of high resolution EEG and fMRI data by Directed Transfer Function," *NeuroImage*, vol. 24, pp. 118-131, 2005.

[7] M. Wagner, M. Fuchs and J. Kastner, "fMRI-constrained dipole fits and current density reconstructions," *Proc 12th Int Conf Biomag*, CD-ROM, 2000.

[8] S. Twomey, "On the numerical solution of Fredholm integral equations of the first kind by the inversion of the linear system produced by quadrature," *J. Assoc. Comput. Mach.*, vol. 10, pp. 97-101, 1963;

[9] Z. Liu, F. Kecman and B. He, "Effects of fMRI-EEG mismatches in cortical current density estimation integrating fMRI and EEG: a simulation study," *Clin. Neurophysiol.*, in press.

[10] A. M. Dale and M. I. Sereno, "Improved localization of cortical activity by combining EEG and MEG with MRI cortical surface reconstruction: a linear approach," *J. Cogn. Neurosci.*, vol. 5, pp. 162-176, 1993.

[11] M. S. Hamalainen and J. Sarvas, "Realistic conductivity geometry model of the human head for interpretation of neuromagnetic data," *IEEE Trans Biomed Eng*, vol. 36, pp. 165-171, 1989.

[12] P. C. Hansen, "Analysis of discrete ill-posed problems by means of the L-curve," *SIAM Rev*, vol. 34, pp. 561-580, 1992.

[13] M. Fuchs, M. Wagner, T. Kohler, H. A. Wischmann, "Linear and nonlinear current density reconstructions," *J. Clin. Neurophysiol*, vol. 16, 267– 295, 1999.

[14] A. M. Dale, A. K. Liu, B. R. Fischl, R. L. Buckner, J. W. Belliveau, J. D. Lewine and E. Halgren, "Dynamic statistical parametric mapping: combining fMRI and MEG for high-resolution imaging of cortical activity," *Neuron*, vol. 26, pp. 55-67, 2000.